Research Square

Preprints are preliminary reports that have not undergone peer review.
They should not be considered conclusive, used to inform clinical practice,
or referenced by the media as validated information.

Glucose-Assisted Synthesis of Hierarchical Zeolite Y for CO_2 Capture: Adsorption Isotherms, Selectivity, and Isosteric Heat

HAMZA ASMALY
King Fahd University of Petrolum and Minerals
Bakae Idris
King Fahd University of Petrolum and Minerals
Nusiba M Alshik
Mansur Aliyu
King Fahd University of Petrolum and Minerals
Amani Chrouda
amain.c@mu.edu.sa

Research Article

Keywords:

Posted Date: November 24th, 2026

DOI: https://doi.org/10.21203/rs.3.rs-11569095/v1

License: This work is licensed under a Creative Commons Attribution 4.0 International License.
Read Full License

Additional Declarations: No competing interests reported.

Glucose-Assisted Synthesis of Hierarchical Zeolite Y for CO_2 Capture: Adsorption Isotherms, Selectivity, and Isosteric Heat

Abstract

In this study, a glucose modified hierarchical Zeolite Y adsorbent was developed for high-performance CO_2 capture. Glucose as a soft templating agent was used to modify the pore structure and surface chemistry for preparing the multifunctional adsorbent with improved adsorption performance. The synthesized materials were characterized by XRD, FTIR, TGA, SEM-EDX and N_2 adsorption-desorption analysis. Results confirmed the retention of the crystalline zeolite Y structure after modification and the successful introduction of additional oxygen-containing surface functionalities and improved pore accessibility. The unmodified zeolite had the highest BET surface area (862 $m^2.g^{-1}$). The modified samples (with slightly lower surface areas) exhibited better adsorption behavior. The highest CO_2 adsorption capacity was observed for the glucose modified zeolite YS/0.2 of 4.88 $mmol.g^{-1}$ at 273 K and 4.52 $mmol.g^{-1}$ at 298 K in comparison with the unmodified zeolite, which was 3.65 and 3.15 $mmol.g^{-1}$, respectively. Moreover, the CO_2/N_2 selectivity of the YS/0.2 was still high at 11.08 and 11.63 for CO_2/N_2 and 5.34 and 7.91 for CO_2/CH_4 at 273 and 298 K, respectively. The raw zeolite showed the highest heat of adsorption (27.53 $kJ.mol^{-1}$). The YS/0.2 showed the highest of CO_2 uptake due to the improvement of pore accessibility and mass transfer characteristics. The CO_2 adsorption data were well described by the Langmuir model (R^2 = 0.986) and the predicted monolayer capacity (5.15 $mmol.g^{-1}$) was close to the experimental uptake (4.88 $mmol.g^{-1}$) indicating adsorption on relatively uniform sites. The adsorption followed the Freundlich model (R^2= 0.959) indicating adsorption on a heterogeneous surface and the Toth model gave the best overall fit (R^2= 0.999) and confirmed the heterogeneous nature of the adsorption. The results indicate that the glucose-modified adsorbents are multifunctional, simple, cheap and sustainable for carbon capture.

Keywords: Glucose; Zeolite Y; Hierarchical porosity; Sustainable Adsorbents; CO_2 capture.

Nomenclature

SN	Abbreviation	Full Term
1	Zeolite Y	Faujasite Y (FAU-Y) Zeolite
2	YS	Y-Type Zeolite/Silica Composite
3	YS/0.2	Y-Type Zeolite/Silica Composite Modified with 0.2 Composition Ratio of Glucose
4	YS/0.5	Y-Type Zeolite/Silica Composite Modified with 0.5 Composition Ratio of Glucose.
5	Na-LTA Zeolite	Sodium Linde Type A Zeolite
6	Na-FAU Zeolite	Sodium Faujasite Zeolite
7	AMS-Z13X	Amine-Modified Sodium Zeolite 13X (FAU Structure)
8	Z- 5A	Calcium-Exchanged Linde Type A (5A) Zeolite
9	Na-A Z	Sodium Linde Type A (NaA) Zeolite
10	H-ZSM-5	Hydrogen Form of Zeolite Socony Mobil-5
11	Zeolite ZSM-5	Zeolite Socony Mobil-5
12	TMAOH	Tetramethylammonium hydroxide
13	TPAOH	Tetrapropylammonium hydroxide
14	TEPA	Tetraethylenepentamine
15	MOR	Mordenite framework type of zeolite
16	PSD	pore size distribution

Highlights

- The synthesis driven by glucose resulted in a hierarchical pore structure and increased the CO_2 uptake from 3.65 to 4.88 mmol.g^{-1}.
- The isosteric heats of adsorption (ranging from 13.45 to 27.53 kJ.mol^{-1}) show that the capture of CO_2 is governed by physisorption and is therefore favorable.
- The high selectivities for CO_2 over N_2 and for CO_2 over CH_4 mean that the modified zeolites are suitable for use in the industrial separation of gases.
- The experimental uptake value of 4.88 mmol.g^{-1} is very close to the Langmuir capacity of 5.18 mmol.g^{-1}, which shows that the adsorbents are reliable.

1. INTRODUCTION

Industrial developments have led to an escalation in greenhouse gas emissions on a global scale. Carbon dioxide (CO_2) is one of the most prevalent greenhouse gases, and emissions of which have been enhanced by anthropogenic activities such as the combustion of fossil fuels and deforestation, leading to climate change and environmental damage [1-4]. The enhanced levels of CO_2 in the atmosphere have intensified the greenhouse effect, causing global warming, sea level rise, change in weather pattern, and extreme climate events such as droughts, heat waves, and severe storms [5-10]. Additionally, a significant amount of the CO_2 emitted is absorbed in the oceans, causing ocean acidification, which is detrimental to marine life and the overall ecosystem [11-13]. Thus, there is a need to reduce greenhouse gas emissions for the betterment of the global environment [14].

CO_2 can be captured from industrial effluents and directly from the atmosphere through various techniques such as absorption [15, 16], adsorption [17, 18], cryogenic distillation [19, 20],

membrane separation [21, 22], and oxy-fuel combustion [23-25]. However, these processes are energy-intensive and require high operating costs, complex technology, and regeneration [26, 27]. Therefore, there is a need to develop cost-effective and efficient materials and processes to capture CO_2 from the atmosphere.

Adsorption is a simple process that can be easily regenerated and require less energy. A variety of materials such as carbon-based materials, metal-organic frameworks, mesoporous materials, and zeolites have been explored as promising adsorbents for CO_2 capture [28-30]. Zeolites are a class of aluminosilicates with a microporous structure and have shown potential as adsorbents for CO_2 capture due to their unique characteristics such as the ability to selectively interact with CO_2 molecules and thermal stability [31]. In particular, Zeolite Y has been considered as a potential candidate for CO_2 capture due to its high surface area and porous structure which facilitate a higher CO_2 uptake due to the presence of multiple adsorption sites [31–33]. The key characteristics of Zeolite Y that make it a potential candidate for CO_2 capture are its microporosity, CO_2 selectivity, regenerability, reusability, and operability at different pressures, temperatures, and humidity levels [34, 35]. Its selectivity makes it appropriate for CO_2 separation or purification from a mixture of gases [36]. Additionally, Zeolite Y can be regenerated and reused since it has been observed to retain its adsorption capacity after multiple cycles of adsorption and desorption [37, 38]. The adsorption of CO_2 on Zeolite Y has been observed to be dependent on the pressure and temperature; higher pressure and lower temperature enhance the adsorption of CO_2 on Zeolite Y [36]. However, Zeolite Y has a slower diffusion rate and a comparatively smaller pore size, limiting its ability to selectively capture CO_2.

In this study, the structure of GO was engineered using glucose as a template to develop new materials with enhanced adsorption capacity and diffusion rate. The fabricated structure was used

to modify the pores of Zeolite Y to increase its adsorption capacity for CO_2. It was hypothesized that the modification of Zeolite Y using the newly created GO with glucose as a template would result in a material with enhanced CO capacity. As a natural and renewable polymer, glucose can be used as a soft template to fabricate a micro-mesoporous structure without destroying the crystallinity of Zeolite Y (Figure 1). The newly created pores in Zeolite Y will provide an efficient adsorption pathway and promote faster diffusion of CO_2 molecules into the interior of the material. As a result, the adsorption capacity of Zeolite Y would be enhanced. Therefore, this study aimed to fabricate a modified form of Zeolite Y that could be used in CO_2 capture and reduce the emission of greenhouse gases.

2. MATERILAS AND METHODS

2.1 Materials and Chemicals

Zeolite Y was created in this study using reagents that're of analytical grade. Glucose was used as a template to change Zeolite Y and create a structure with different sized pores. This structure helps Zeolite Y to absorb substances. The synthesis reagents included sodium aluminate (Na Al_2O_3, Sigma-Aldrich) as the aluminum source, colloidal silica HS-40 (40 wt.% SiO_2 suspension, Sigma-Aldrich) as the silicon source, sodium hydroxide (NaOH, Honeywell), hydrochloric acid (HCl, 37 wt.%, Carlo Erba), and deionized water. Additionally, chemicals used for sample preparation, pH adjustment, and adsorption experiments included sodium hydroxide (NaOH), and acetone (C_3H_6O, 98% purity). All chemicals were of analytical grade and were used as received without further purifications. Liquid Nitrogen used for the analysis of the surface area of the samples, High purity gases used for adsorption measurements were carbon dioxide (CO_2, 99.995%), nitrogen (N_2, 99.996%), and methane (CH_4, 99.998%), which were supplied by a local vendor in Dammam-Saudi arabia.

2.2 Methods

2.2.1 Synthesis of Zeolite Y

In a typical synthesis procedure for refence zeolite Y (mole ratios; 1 Al_2O_3: 14.6 SiO_2: 254.7 H_2O:22.8 NaOH) considering a 60 g basis of all reagent. To start with, 7.6 g of NaOH was dissolved under continuous stirring in 20 ml H_2O in a 100 ml Duran bottle. Thereafter, 1.5 g of $NaAl_2O_3$ was added to the solution and the whole solution was kept under continuous stirring. After 10 minutes, 20 g of colloidal silica HS-40 was added to the solution in a dropwise manner to make solution (A). Next, 11.46 µL of 37 wt.% HCl was dissolved in 10 ml to form solution (B). Solution B was added in drops to solution A under constant stirring. The final solution was kept to age for 20 minutes. Thereafter, the whole solution was tightly covered and transferred into an oil bath a stirrer plate preheated at 95 ^oC. The sample was left for 12 h under constant stirring at 300 rpm. Afterwards, the resulting zeolite was washed several times with hot water until pH of solution becomes 8. The result zeolite was then dried at 100^oC for 12h and calcined at 350^oC for 2h (5 ^oC/min) and then at 500 ^oC for 3h (5 ^oC/min) using a single temperature program in a muffle furnace (Figure 1).

2.2.2 Glucose mediated synthesis (GMS)

In the GMS approach (mole ratios; 1 Al_2O_3: 14.6 SiO_2: 254.7 H_2O: 22.8 NaOH: (0.12-0.30) $C_6H_{12}O_6$), the preparation procedure followed the same steps described previously in paragraph (2.2.1). The only difference is that we added different amounts of glucose before aging the zeolite precursor gel. During the course of synthesis, we added 0.2g and 0.5g of glucose to prepare to separate samples. The Glucose (Soft Templating Agent) plays a significant role in zeolite synthesis as a soft templating agent and microporosity promoter. Incorporating glucose into the synthesis of Y-type zeolites significantly enhances their overall sorption performance. During the

crystallization process glucose molecules work as guides by taking up the spaces between crystals and the areas between building blocks. When the material is then heated, the breaking down of the glucose forms small holes that are between 2 and 50 nanometers in size. This leads to a structure that has levels of holes. It mixes both small holes and medium-sized holes inside the zeolite structure. Because of this structure it helps things move through faster. Makes it easier for molecules to get in by cutting down on the problems, with moving through the material.

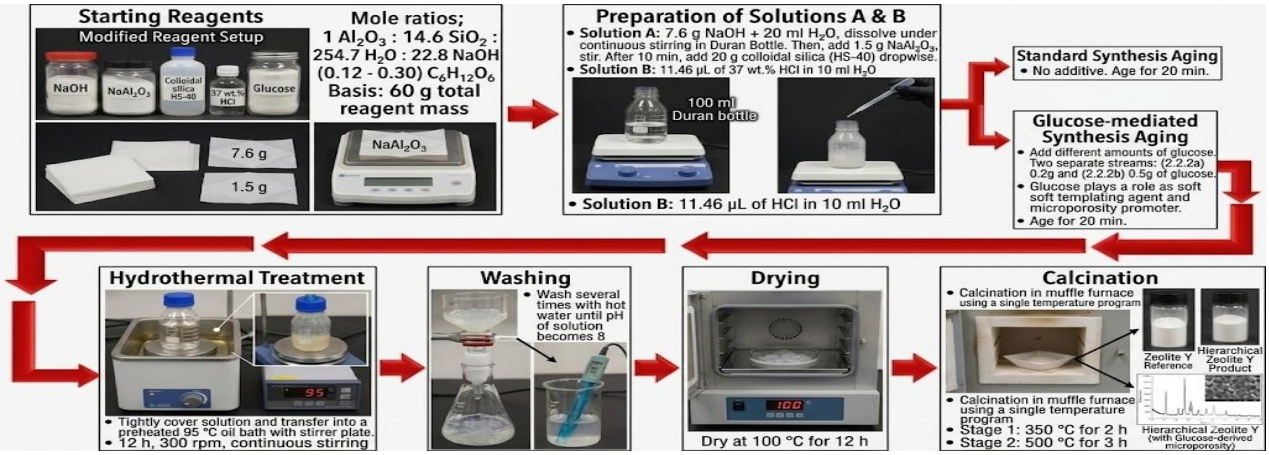

Figure 1. Skeleton of the synthesis and Glucose-assisted modification of Zeolite Y.

2.2.3 Gases Adsorption, Thermodynamics, and Selectivity Analysis

CO_2 and CH_4 adsorption studies were performed to evaluate the performance of the newly synthesized zeolite Y adsorbents for CO_2 capture and gas separation. CO_2, CH_4, and N_2 adsorption isotherms were measured using a QuadraSorb evo surface area and pore size analyzer (version 6) to determine the adsorption capacity of each zeolite Y sample toward the three gases.

Measurements were taken at 0.0° and 25.0°C, at 1 atm each to determine how temperature would affect CO_2 and CH_4 adsorption on zeolite Y. Prior to experimentation, the Y samples were vacuum degassed at 300°C for 8 hours to remove any water and other residual species that may have been adsorbed on the sample. High purity gases were used throughout experimentation to ensure accuracy and reproducibility of data. Pressure-dependent uptake was measured across the entire

pressure range to generate equilibrium isotherms. Amounts adsorbed for CO_2, CH_4, and N_2 were calculated using the instrument software. To determine the energetics of the adsorption process, the isosteric heat of adsorption (ΔH_{ads}) was calculated for CO_2 to determine the efficiency of Y for CO_2 capture and determine the potential operating costs of this process. Adsorption enthalpy was calculated from two isotherms measured at different temperatures using the Clausius–Clapeyron equation (Eq. 1). The Clausius–Clapeyron equation allows ΔH_{ads} to be found by measuring the slope of the line of a plot of ln P vs. 1/T at a constant gas loading.

$$\Delta \mathrm{H_{ads}} = -R \left[\frac{\partial \ln P}{\partial \left(\frac{1}{T}\right)} \right]_q \quad (1)$$

where ΔH_{ads} is the isosteric heat of adsorption ($kJ.mol^{-1}$), R is the universal gas constant, P is the equilibrium pressure, and T is the absolute temperature. The derivative is taken at a constant adsorption uptake q. For each adsorption loading, ln(P) was plotted against 1/T, and ΔH_{ads} were obtained from the slope of the linear relationship [39] as represented in equation (Eq. 2)

$$\ln P = -\frac{\Delta H_{ads}}{R}\left(\frac{1}{T}\right) + \mathrm{A} \quad (2)$$

In addition, the selectivity of CO_2 over CH_4 and N_2 was evaluated to assess the separation performance of the adsorbents. Selectivity was estimated based on the ratio of adsorption capacities at identical conditions according to Ideal Adsorbed Solution Theory (IAST) [39], expressed in equation (3&4) and also calculated according to Henry's law [40] equation (5 &6),

$$S_{\left(CO_2/CH_4\right)} = \left(Q_{\mathrm{CO_2}} \Big/ Q_{\mathrm{CH_4}}\right) \quad (3)$$

$$S_{\left(CO_2/N_2\right)} = \left(Q_{\mathrm{CO_2}} \Big/ Q_{N_2}\right) \quad (4)$$

where $q_{\mathrm{CO_2}}$, $q_{\mathrm{CH_4}}$, and $q_{\mathrm{N_2}}$ represent the adsorption capacities of CO_2, CH_4, and N_2, respectively.

$$S_{\left(CO_2/CH_4\right)} = \left(\frac{K_{H,CO2}}{K_{H,CH4}}\right) \quad (5)$$

$$S_{\left(CO_2/N_2\right)} = \left(\frac{K_{H,CO2}}{K_{H,N2}}\right) \quad (6)$$

KH_{CO2} and KH_{CH4}, KH_{N2} = Henry's constants obtained from the initial slope of the adsorption isotherms of CO_2, CH_4 and N_2, respectively.

The experiments have been reproducibly performed under controlled conditions. This enables not only determination of adsorption capacities, thermodynamic properties and selectivities of gases but also allows to qualitatively conclude about the performance of zeolite Y adsorbents for CO_2 separation and purification applications.

2.2.4 Isotherm Models of CO_2

Zeolite application is very promising for CO_2 capture, owing to their high surface area. Microporosity characteristics of their crystalline structure and the strong affinity of these materials for the CO_2 molecule facilitate their implementation in CO_2 capture processes. The mechanisms of CO_2 adsorption on Zeolites can be modelled using either the Langmuir or the Freundlich isotherms. The former assumes a monolayer coverage of the adsorbate on a homogeneous surface, while the latter considers an adsorbent with heterogeneous sites. Zeolites do not exhibit a particular uniformity in their structure, which makes it necessary to use advanced multi-site models such as the Sips and the dual-site Langmuir in order to properly characterize their adsorption isotherms (Table 1). The models were fitted to the experimental data, and the resulting parameters are reported in Results Section 3.2.4.

Table 1. CO_2 Isotherm Models

Model	Equation	Model Type	Parameter Description
Langmuir	$Q_e = Q_m \frac{K_L P_e}{1 + K_L P_e}$	Linear	P_e (bar): equilibrium pressure; Q_e (mmol/g): adsorbed amount; Q_m (mmol/g): maximum adsorption capacity; K (bar^{-1}): Langmuir constant (affinity)

Freundlich	$Q_e = K_f\left(p_e^{\frac{1}{n}}\right)$	Linear	K_F (mmol/g·bar$^{-1/n}$): adsorption capacity constant; 1/n: adsorption intensity factor; P_e (bar): equilibrium pressure.
Toth	$Qe = \frac{q_{m\,KC_e}}{[1+(KC_e)^t]^{1/t}}$	Non-Linear	P_e (bar): equilibrium pressure of CO_2; q_e (mmol/g): amount of CO_2 adsorbed at equilibrium. q_m (mmol/g): maximum adsorption capacity; K(bar^{-1}): Toth equilibrium (affinity) constant; t: heterogeneity parameter.

2.2.5 Characterization Techniques

The crystallinity of the porous Zeolite adsorbents was assessed via X-ray diffraction (XRD), using a Miniflex II diffractometer from Rigaku. This process entailed specific settings, including an analysis with Cu Kα radiation (λ = 1.5405Å), an X-Ray Generator of 40 kV and 15 mA, a step width of 0.03°, Scan range 0 ~ 90, and scan speed for 3/ min. To examine the samples using a High-Resolution Scanning Electron Microscope (SEM) from the Czech Republic. The elemental composition of these samples was then studied using Energy Dispersive X-ray Spectroscopy (EDX). Nitrogen adsorption/desorption isotherms, captured at a temperature of 77 K using a Surface Area and Porosity Analyzer Micromeritics model ASAP2020, were used to identify the surface area. All samples were degassed for 6 hours at 120°C prior to measurement. Specific surface area was measured by the Brunauer-Emmett-Teller (BET) method. Pore size distribution (PSD) and the micropore and mesopore volumes were derived using Barrett-Joyner-Halenda (BJH) theory, which together describe the pore structure governing CO_2 diffusion and uptake. FTIR spectra were recorded on a Nicolet FT-IR 6700 spectrophotometer..

3. RESULTS AND DISCUSSION

3.1 Adsorbents Characterization

3.1.1 BET Surface Area and Pore size distribution Analysis

The N_2 adsorption-desorption isotherms of YS, YS/0.2, and YS/0.5 (Figure 2) exhibit Type-IV behavior with H4-type hysteresis loops, confirming the presence of hierarchical micro-mesoporous structures. All samples showed a sharp increase in nitrogen uptake at low relative pressures, indicating significant microporosity, followed by gradual adsorption at higher relative pressures due to capillary condensation within mesopores. The pristine zeolite (YS) exhibited the highest BET surface area (862 $m^2.g^{-1}$), whereas YS/0.5 and YS/0.2 showed slightly lower values of 780 and 769 $m^2.g^{-1}$, respectively. These values remain comparable to those reported for Zeolite Y in the literature (727 $m^2.g^{-1}$) [43], confirming that glucose modification preserved the highly porous zeolitic structure. The reduction in surface area suggests that part of the original microporous network was partially occupied or restructured during glucose-assisted synthesis. In spite of this fact, glucose incorporation led to the growth of additional mesoporosity and better interconnectivity of pores, resulting in a more developed hierarchical pore system. This result was particularly advantageous for YS/0.2 as it exhibited the highest CO_2 uptake despite the fact that the BET surface area of it is slightly lower than that of YS/0.5. Performance of YS/0.2 suggests that in addition to the total surface area the CO_2 uptake is affected by pore structure and availability and diffusional paths. Moderate glucose loading (0.2 g) seems to ensure a good trade-off between microporosity and mesoporosity and makes it possible to create efficient transport pathways that let the gas diffuse quickly into the internal sorption sites and maintain strong interaction with zeolite. On the other hand, the more significant glucose amount could have led to partial pore

blocking or excessive modification of pore system structure, decreasing the availability of active sorption sites.

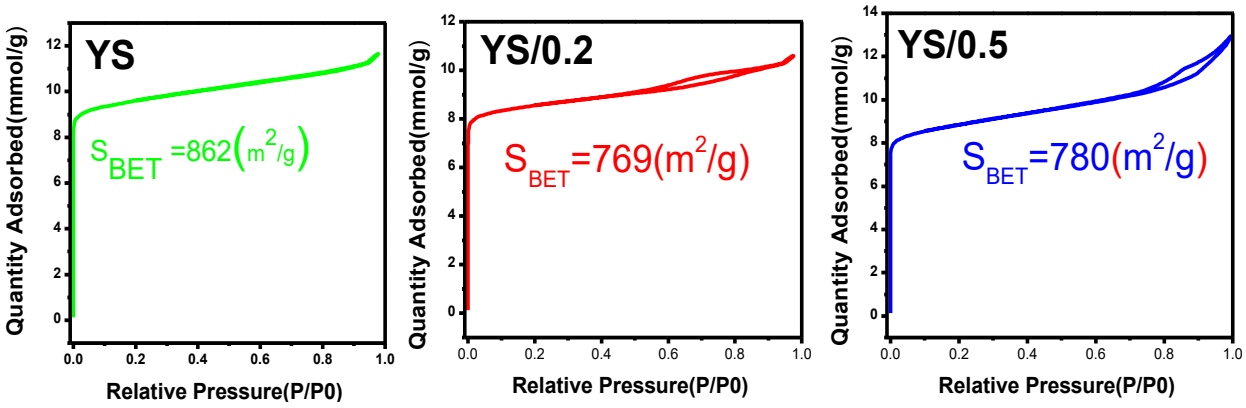

Figure 2. N_2 absorption/desorption Isotherm of three variations of Zeolite-Y.

The PSD graphs shown in Figure 3 for all the three samples YS, YS/0.2 and YS/0.5 display a hierarchical porous structure having micropores as the dominating pore system with some additional contributions being present in the mesopore region. The presence of a peak in the interval of 0-5 nm supports the suitable modification of zeolite Y done by the glucose. On the other hand, the analysis of all zeolite Y samples provides evidence for a significant influence of the residues derived from glucose carbonaceous compound because the YS/0.2 sample displays pores that are characterized by a good access of CO_2 molecules to the active sites, while in the case of YS/0.5 sample it can be observed that the volume has become restricted, which might indicate overloading and incomplete filling up of channels in zeolite Y. This suggests some kind of balance between practical usage of the porous system and its ability to function properly with YS/0.2 being the ideal sample compared to non-functional YS and over-restricted YS/0.5 sample.

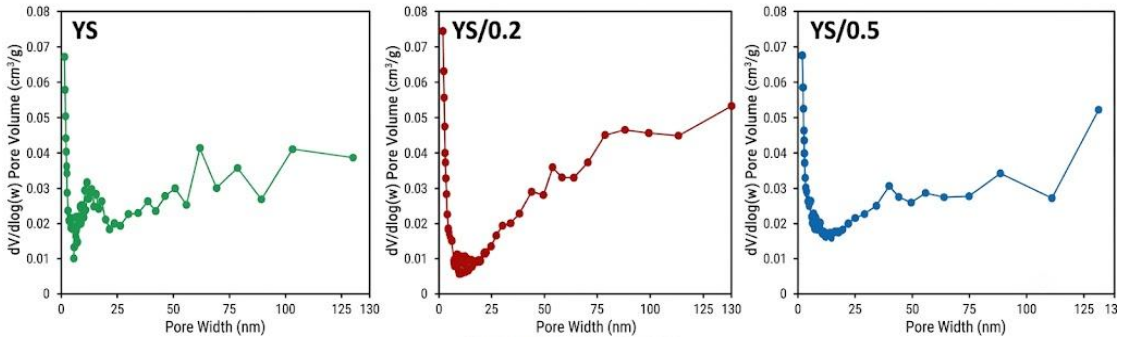

Figure 3. BJH Adsorption pore size distributions of the Three types of Zeolite-Y.

3.1.2 BET and PSD Analysis and Correlation with CO_2 Uptake

The result of the BET and PSD analysis, summarized in Table 2, showed that the paper discusses how the textural and adsorption data relate to the synthesized samples. The data reveal a trend that while the main YS zeolite (without modifications) has the largest BET surface area (862 $m^2.g^{-1}$), the glucose-modified samples serve as better CO_2 adsorbers. This indicates that there is a somewhat obvious trade-off between the structural surface area of the material and the chemically active functionalization it contains. A close look at the adsorption results under realistic conditions reveals that the YS/0.2 sample exhibits the highest CO_2 storage capacity of 4.885 mmol. g^{-1}, which can be ascribed to its highest pore volume of 0.435 mmol. g^{-1} and a pore width of 3.041 nm that is almost the same as in the pristine YS so as to accommodate the gas molecules. On the other hand, the YS/0.5 sample did not only have its CO_2 uptake capacity increased to 4.699 mmol. g^{-1} but was also able to increase the average pore volume up to 0.326 cm^3. g^{-1}, unlike the case of the original YS where it is only 3.651 mmol. g^{-1}. The impact of the decreased pore volume (0.326 cm^3. g^{-1}) and the pore width becoming narrower (2.756 nm) is the decline in the performance of the YS/0.5 relative to the YS/0.2 given that a molecule of a larger size (i.e. radius) has to find its way through fewer channels. This means the discipline that the framework of the YS/0.2 offers in the regions where the chemical functionalities are introduced by means of glucose is orthogonal to the one where pure and structurally restricted YS is situated, and this is the major reason for the attainment

of the maximum adsorption efficiency through the combination of the hierarchical zeolite architecture and the chemically active functionalization. In essence, the YS/0.2 shows the most effective union between the hierarchical structure of the zeolite and the introduced chemical functionality, thus, leading to the highest adsorption capacity in comparison with both the inert pristine framework and the structurally constrained YS/0.5.

Table 2. Differences in the texture and CO_2 adsorption efficiency of Zeolite Y before and after glucose modification

Sample	BET ($m^2.g^{-1}$)	Pore width (nm)	Pore volume ($cm^3.g^{-1}$)	CO_2 uptake (mmol. g^{-1})
YS	862	3.047	0.428	3.651
YS/0.2	769	3.041	0.435	4.885
YS/0.5	780	2.756	0.326	4.699

3.1.3 Thermal Gravimetric Analysis (TGA)

Figure 4(a) shows the TG profiles of the non-thermally treated zeolite (YS) and the glucose-treated samples (YS/0.2 and YS/0.5). Interestingly, all samples followed a similar pattern typical of thermal decomposition: a first stage of minor weight loss at lower temperatures, followed by a relatively stable region at higher ones, thus confirming the high thermal stability of the synthesized zeolites. The first weight loss below about 150-200°C is mostly due to the removal of physically adsorbed water ,molecules as well as residual moisture captured in the pores of the zeolite. Since aluminosilicate materials are quite hygroscopic and have a high affinity for water molecules, this type of behavior is quite expected. The samples treated with glucose demonstrated slightly higher weight losses compared to the unmodified zeolite, pointing primarily to the decomposition of residual glucose-derived carbonaceous species incorporated during the synthesis. The bigger weight loss seen in YS/0.5 and YS/0.2 points to the fact that more glucose was used during the synthesis. The minimal additional weight loss at temperatures higher than 450°C, which was

observed in all samples, speaks to their very high thermal stability and the intactness of the Zeolite Y framework. The data obtained here lead to the conclusion that the glucose -assisted synthesis was an effective approach for the generation of a hierarchical pore structure without losing the thermal integrity of the zeolite. The better pore accessibility brought about by glucose decomposition is thought to be the reason behind the enhanced CO_2 adsorption of the modified zeolite samples.

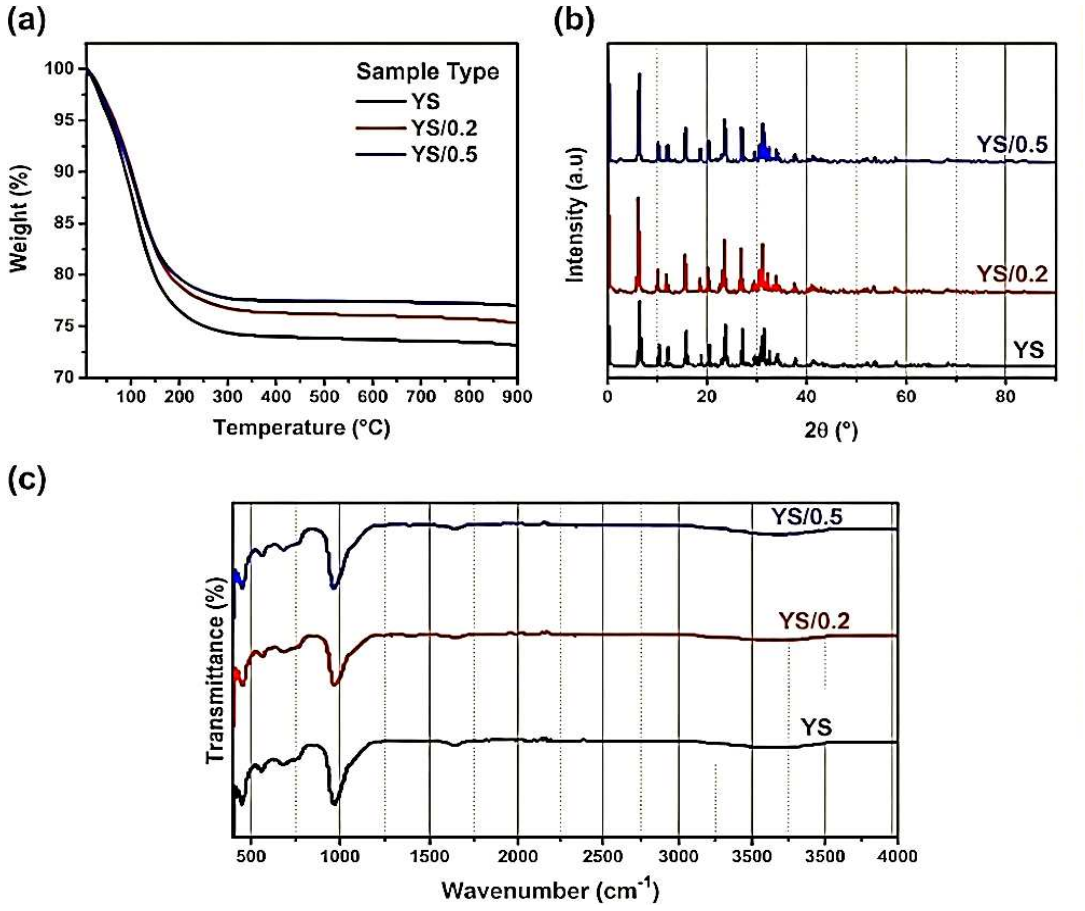

Figure 4. Comprehensive characterization of YS series via **(a)** TGA, **(b)** XRD, and **(c)** FTIR analyses

3.1.4 X-Ray Diffraction (XRD)

Figure 4(b) presents the XRD patterns of YS, YS/0.2, and YS/0.5. All the samples show the typical diffraction peaks of Zeolite Y, which confirms that Zeolite Y was successfully synthesized in a

crystalline form. The sharp and intense peaks reveal a high level of crystallinity and the presence of a well-ordered structure. The main diffraction peaks did not change after glucose modification, indicating that the inclusion of glucose did not affect the core crystal structure of the zeolite. Moreover, from spectroscopic data there were not observed any peaks attributed to impurity phases, hence confirming the purity of the prepared samples. In the case of glucose-modified samples (particularly YS/0.5) a slight decrease in the intensity of peaks was observed which corresponded possibly with formation of hierarchical porosity and minor structural changes occurring during calcination. However, the overall level of crystallinity for glucose-modified samples remained at a similar level and with a similar structure as reported by [43]. Such observations suggest that the glucose-assisted synthesis technique allowed the formation of hierarchical Zeolite Y preserving the crystalline zeolitic framework and structural integrity of obtained materials.

The retained crystallinity and the increased pore accessibility, in combination, are likely to be the reasons behind the higher CO_2 adsorption performance detected for the modified samples.

3.1.5 FTIR

The FTIR spectra of the glucose-modified Zeolite Y samples (YS/0.2 and YS/0.5) as shown in Figure (4c) exhibit the characteristic vibrational bands of the Zeolite Y aluminosilicate structure, together with additional absorption bands associated with glucose - derived surface functional groups. Both samples show a strong and broad absorption in the region of 3400-3450 cm^{-1}, corresponding to O-H stretching vibrations from surface hydroxyl groups and adsorbed water, with YS/0.5 displaying a noticeably higher intensity, indicating the presence of more abundant hydroxylated sites generated during glucose modification. The bands observed near 1630-1650 cm^{-1} are attributed to H-O-H bending vibrations of physiosorbed water. The dominant framework

vibrations appear in the 1000-1100 cm^{-1} region, associated with asymmetric stretching of Si-O-Si and Si-O-Al linkages, confirming that the primary zeolite structure remains intact after functionalization. Additional features in the 1350-1450 cm^{-1} region can be assigned to the C-O and C-H deformation modes produced by the glucose-derived species residual, with the increased intensity for YS/0.5 being caused by higher surface functionalization. The bands of 450-800 cm^{-1} are characteristic of T-O bending modes (T = Si or Al), which indicate that the crystalline aluminosilicate network was preserved in the samples. A similar pattern was also described in the work [43], which also proved that the crystalline framework of the zeolite was preserved, and the Si/Al ratio had a significant influence on the obtained materials' structural properties that were synthesized. Bands of O-H and those related to carbon in YS/0.2 and YS/0.5 were more intense, denoting that the surface functionalization was more pronounced, leading to the increased surface polarity, and, hence, a greater number of active adsorption sites. These results perfectly match the BET and TGA data, which further verify the enhanced adsorption capacity of the glucose-modified zeolites in comparison to the unmodified YS sample.

3.1.6 SEM–EDS

The SEM images of YS, YS/0.2, and YS/0.5 are quite similar. All these samples show aggregations of zeolite crystals with irregular particle assemblies. This is also depicted in Figure 5. After glucose modification, there was no notable structural collapse or major morphological changes. This suggests that the particle structure of Zeolite Y was retained in the synthesis and calcination processes. The modified samples maintained the characteristic morphology of Zeolite Y, indicating that the crystalline zeolitic structure remained intact after glucose modification, as confirmed by the XRD results presented in Figure 4(b). Therefore, the improved adsorption performance observed for the modified samples cannot be attributed to substantial morphological

changes but rather to modifications in surface chemistry and pore accessibility. The EDX spectra (Figure 4) were used to investigate the elemental composition of the unmodified and glucose-modified zeolites and to evaluate the effect of glucose incorporation on the zeolite surface. All samples exhibited the characteristic framework elements of Zeolite Y, namely O_2, Si, and Al, and Na, confirming the preservation of the aluminosilicate structure after modification as detailed below in Table 3. The unmodified zeolite (YS) exhibited O_2, Si, and Al contents of 36.47, 18.65, and 11.26 wt %, respectively, together with a carbon content of 22.66 wt%. Following glucose modification, a noticeable increase in carbon content was observed, reaching 29.00 wt %for YS/0.2, accompanied by slight reductions in Si and Al and contents. This increase indicates the successful incorporation of carbonaceous species derived from glucose to the surface of the zeolite, and suggests the formation of more oxygen-rich functional groups. YS/0.5, on the other hand, had a carbon content of 20.30 wt%, which was still in the same range as the unmodified sample albeit lower than that of YS/0.2. The reason for this could be that with higher glucose loading, some of the carbonaceous species got thermally decomposed or burnt out, resulting in a more stable and reorganized surface structure. The fact that both modified samples had high oxygen contents also strongly indicates that the surface functionalities were enriched with oxygen and were a result of glucose-assisted synthesis. Such functional groups can not only serve as extra adsorption sites but also promote the interaction with molecules of the adsorbate. Slight changes in Na content could alternatively be interpreted as a partial redistribution of the extra-framework cations during the synthesis and calcination phases, which might affect the adsorption characteristics. Furthermore, fluorine signals detected in all samples originate from ammonium fluoride used during zeolite synthesis and do not indicate the formation of secondary phases.

Table 3. Chemical Composition of unmodified and Modified Zeolite (Weight Percent)

Element	Carbon	Oxygen	Fluorine	Sodium	Aluminum	Silicon	Total

Symbol	C	O	F	Na	Al	S	
			Weight (%)				
YS	22.66	36.47	2.13	8.83	11.26	18.65	100
YS/0.2	29.00	33.90	3.35	7.67	10.63	16.05	100
YS/0.5	20.30	36.10	3.90	8.67	11.90	19.11	100

The SEM-EDX results indicate that glucose modification preserved the morphology and framework structure of Zeolite Y while enhancing its surface chemistry. Among the modified samples, YS/0.2 exhibited the highest carbon enrichment, suggesting more effective surface functionalization. The introduction of carbon and oxygen containing groups is expected to enhance CO_2 adsorption, which may explain the excellent adsorption performance of YS/0.2 type.

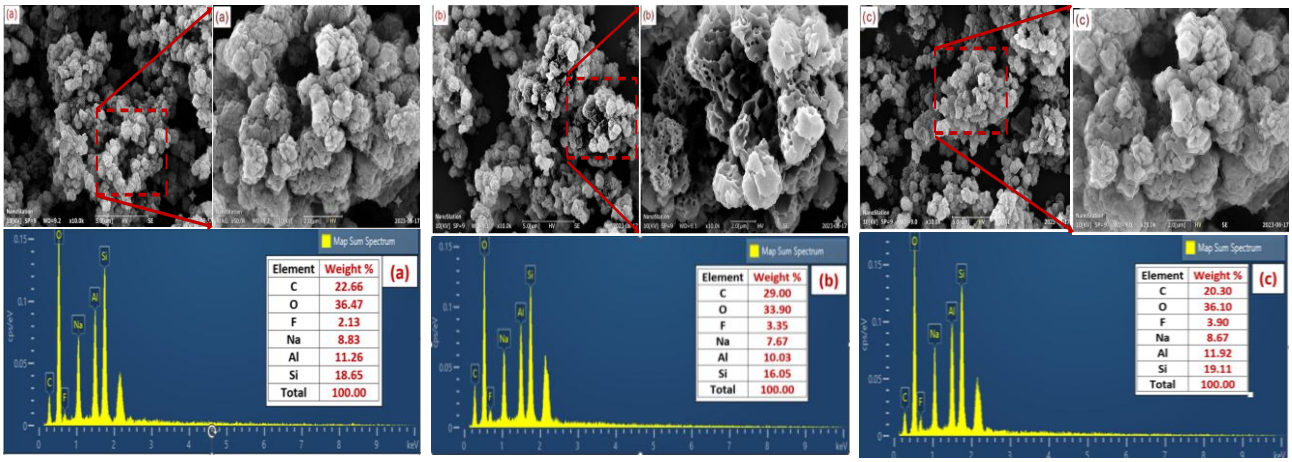

Figure 5. SEM Images & EDX Spectrums of the (a) Zeolite-YS (b) Zeolite-YS/0.2 (C) Zeolite-YS/0.5

3.2 Study on Gases Adsorption

3.2.1 Uptake of CO_2, N_2 and CH_4

The adsorption performance of the unmodified zeolite (YS) and glucose-modified samples (YS/0.2 and YS/0.5) was evaluated for CO_2, N_2, and CH_4 at 273.15 K and 298.15 K, and the results are presented in Table 4 and plotted in Figure7(a, b and c). For CO_2 adsorption, adsorption, the glucose-modified zeolites exhibited significantly enhanced performance compared with the pristine Zeolite Y. At 273.15 K, YS/0.2 achieved the highest CO_2uptake of 4.885 mmol.g^{-1},

followed by YS/0.5 (4.699 mmol.g^{-1}), whereas the unmodified zeolite adsorbed 3.651 mmol.g^{-1}. As expected, the adsorption capacities decreased at 298.15 K due to the exothermic nature of the adsorption process; however, the same trend was maintained, with YS/0.2 and YS/0.5 exhibiting CO_2 uptakes of 4.52 and 4.31 mmol.g^{-1}, respectively, compared with 3.15 mmol.g^{-1} for the unmodified sample. Furthermore, the adsorption performance of the glucose-modified zeolites exceeded that reported in our previous study on highly porous activated carbon, which achieved CO_2 uptakes of 4.61 and 3.00 mmol.g^{-1} at 273 and 298 K, respectively [44]. The improved CO_2 adsorption behavior of YS/0.2 and YS/0.5 can be attributed to the formation of a hierarchical micro-mesoporous structure that enhances pore accessibility, facilitates CO_2 diffusion to internal adsorption sites, and promotes stronger interactions between CO_2 molecules and the zeolitic framework.

Table 4. Gas Adsorption Performance of Unmodified and Modified Zeolite Y Samples at Different Temperatures

Sr	Zeolite	CO_2 Uptake (mmol.g^{-1})		N_2 Uptake (mmol.g^{-1})		CH_4 Uptake (mmol.g^{-1})	
		273 K	**298 K**	**273 K**	**298 K**	**273 K**	**298 K**
1	YS	3.651	3.154	0.251	0.202	0.559	0.344
2	YS/0.2	4.885	4.526	0.441	0.389	0.915	0.572
3	YS/0.5	4.699	4.312	0.418	0.311	0.731	0.396

In the case of the N_2, the adsorption performance showed a completely different trend. The unmodified zeolite (YS) had the highest N_2 uptake across the entire pressure range, with YS/0.2 and YS/0.5 coming next, respectively, as shown in Figure 6 (d, e and f). The decrease in N_2 adsorption after glucose modification indicates that the addition of glucose changed the pore structure and surface properties of the zeolite. Although glucose-assisted synthesis generated a hierarchical micro- mesoporous network, part of the original microporous volume responsible for N_2 adsorption may have been partially transformed or rendered less accessible. Since N_2 adsorption at ambient temperature is primarily governed by micropore accessibility and weak

physisorption interactions, the lower N_2 uptake observed for YS/0.2 and YS/0.5 indicates a reduction in the number of effective adsorption sites available for nitrogen molecules. Similar trend was observed for CH_4 adsorption, where the raw zeolite (YS) exhibited the highest methane uptake, followed by YS/0.2 and YS/0.5 as shown in Figure 6 (g, h and i) respectively. This distinction became more significant at high pressures, demonstrating that glucose modification caused substantial changes in the adsorption mechanism of the zeolite. In contrast to CO_2, methane is a non-polar molecule, where the adsorption is governed primarily by the availability of the micropore volume and the pore-filling effect. Therefore, the partial transformation of the initial microporous structure into a hierarchically porous micro-mesoporous network resulted in a lower number of available adsorption sites for CH_4 molecules. Meanwhile, CO_2 adsorption isotherms benefited from both the micropore filling mechanism and the increased hydrophilicity of the modified zeolite structure that enhanced the electrostatic interaction between CO_2 molecules and the adsorbent. Moreover, the creation of additional mesopores during glucose modification improved CO 2 diffusion inside the porous system.

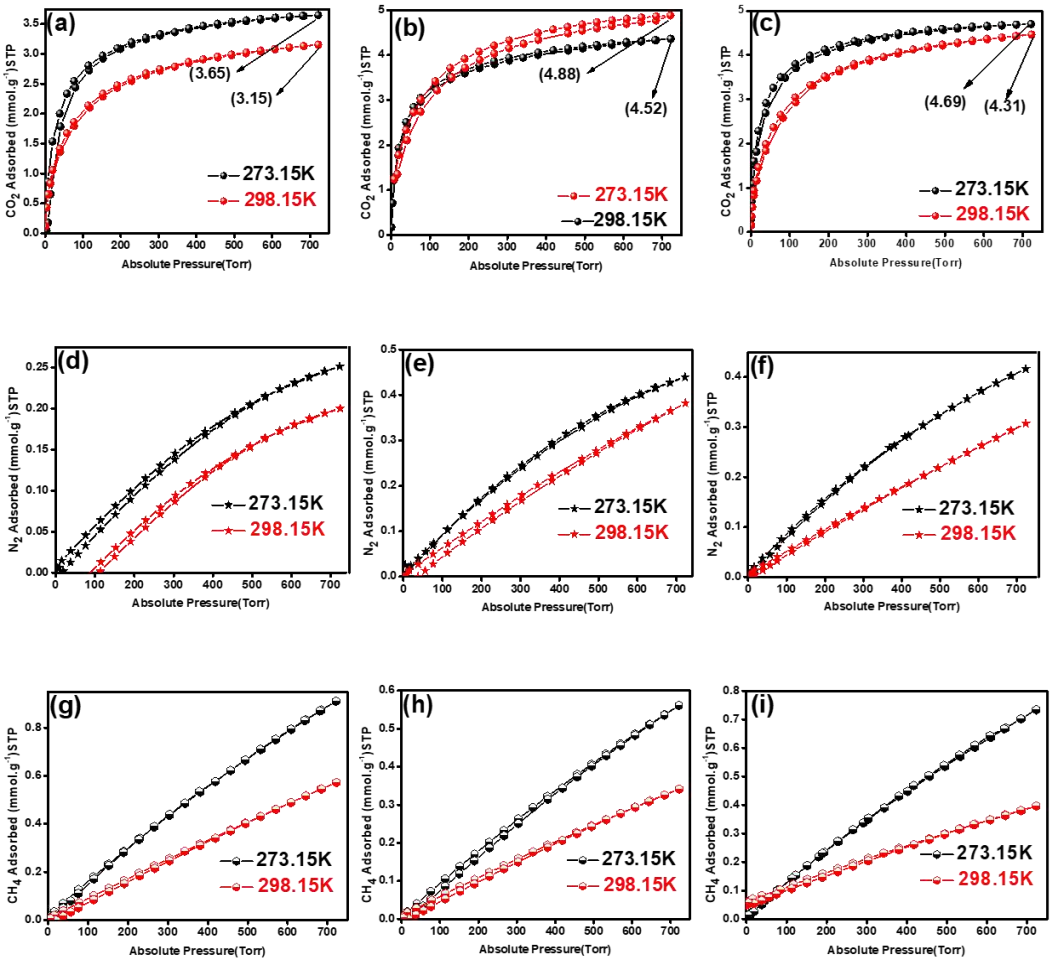

Figure 6. CO_2 adsorption isotherms of (a) YS, (b) YS/0.2, and (c) YS/0.5; N_2 adsorption isotherms of (d) YS, (e) YS/0.2, and (f) YS/0.5; and CH_4 adsorption isotherms of (g) YS, (h) YS/0.2, and (i) YS/0.5 measured at different Temperatures.

In case of N_2 adsorption, the modified zeolites showed higher adsorption capacities than the raw zeolite [Figure 6 (d, e and f)]. The sorption capacity followed the order YS/0.2 > YS/0.5 > YS at both temperatures. At 273 K, the N_2 uptake increased from 0.251 mmol.g^{-1} for YS to 0.441 and 0.418 mmol.g^{-1} for YS/0.2 and YS/0.5, respectively. A similar tendency was observed at 298 K, where both YS/0.2 and YS/0.5 showed higher N_2 uptakes in comparison with the raw zeolite. This fact suggests that glucose modification favored the formation of a hierarchical micro-mesoporous structure that enhances the accessibility of nitrogen molecules into the pores of the zeolite, thus

facilitating its diffusion through the whole framework. The additional porosity created during calcination could be responsible for the increase of the available adsorption sites for nitrogen molecules and the improvement of their diffusion through the material.

A similar trend was observed for CH_4 adsorption as well, which is depicted in Figure 6 (g, h and i). The adsorption capacity was in the order of YS/0.2 < YS/0.5 < YS over the whole pressure range. At 273 K, the CH_4 uptake increased from 0.559 $mmol.g^{-1}$ for YS to 0.915 $mmol.g^{-1}$ and 0.731 $mmol.g^{-1}$ for YS/0.2 and YS/0.5, respectively. Similarly, at 298 K, the modified samples still had higher methane adsorption capacities than the raw zeolite. As methane adsorption is mostly determined by pore-filling mechanisms and the accessible pore volume, the higher CH_4 uptake indicates that the glucose-assisted synthesis brought about improvements in the textural characteristics of the zeolite through the formation of a more accessible hierarchical pore network. The rise in N_2 and CH_4 adsorption that represents the glucose modification as a way of enhancing the overall pore accessibility and mass transfer of the zeolite structure.

3.2.2 Assessment of CO_2 Adsorption Selectivity

3.2.2.1 Ideal Adsorbed Solution Theory (IAST)-Based Selectivity

The selectivity of the synthesized zeolite samples toward CO_2 over N_2 and CH_4 was evaluated from the ratio of their respective adsorption capacities measured under identical conditions. A similar approach for selectivity assessment was previously reported in our earlier study [58, 59]. The calculated selectivity values are summarized in Table 5. At 273 K, the unmodified zeolite (YS) showed the highest CO_2/N_2 selectivity of 14.55, with YS/0.5 (11.24) and YS/0.2 (11.08) following it. In the same way, the CO_2/CH_4 selectivity values were 6.53, 6.43, and 5.34 for YS, YS/0.5, and YS/0.2, respectively. At 298 K, the selectivity values increased considerably, with YS exhibiting the highest CO_2/N_2 selectivity of 15.61 and CO_2/CH_4 selectivity of 9.16. The YS/0.5

sample maintained relatively high selectivity's of 13.86 and 10.89 toward N_2 and CH_4, respectively, whereas YS/0.2 showed the lowest selectivity values. The enhanced selectivity toward CO_2 compared with N_2 and CH_4 can be attributed to the stronger interaction between CO_2 molecules and the zeolite framework. Since CO_2 has a greater quadrupole moment and polarizability than N_2 and CH_4, it interacts more strongly through electrostatic forces with the adsorption sites inside the zeolite structure. Although glucose modification enhanced the overall CO_2 adsorption capacity (particularly for YS/0.2 and YS/0.5 at 273 K), it did increase the adsorption of N_2 and CH_4 to a certain extent, resulting in slightly lower selectivity values when compared to the parent zeolite. However, the modified samples showed significantly higher CO_2 uptake capacities with favorable selectivity, demonstrating the beneficial effect of glucose-assisted synthesis on the development of hierarchical zeolite adsorbents for CO_2 capture.

Table 5. Calculated CO_2/N_2 and CO_2/CH_4 adsorption selectivity's of unmodified and modified Zeolite Y samples at different temperatures

Zeolite Type	CO_2 (mmol. g^{-1})	N_2 (mmol. g^{-1})	CH_4 (mmol. g^{-1})	CO_2/N_2 Selectivity	CO_2/CH_4 Selectivity
			273K		
YS	3.651	0.251	0.559	14.55	6.53
YS/0.2	4.885	0.441	0.915	11.08	5.34
YS/0.5	4.699	0.418	0.731	11.24	6.38
			298K		
YS	3.154	0.202	0.344	15.61	9.16
YS/0.2	4.526	0.389	0.572	11.63	7.91
YS/0.5	4.312	0.311	0.396	13.86	10.89

3.2.2.2 Henry's Law-Based Selectivity

The CO_2 adsorption selectivity of the unmodified and glucose-modified zeolite samples was determined using the Henry's Law, based on Equations (5) and (6). By plotting the initial adsorption isotherm data for each gas at two different Temperatures in the low-pressure region as shown in Figure 7, the Henry's constants were derived from the slope of the linear regression, which represents the intrinsic adsorption affinity of the zeolite framework toward the guest molecules.

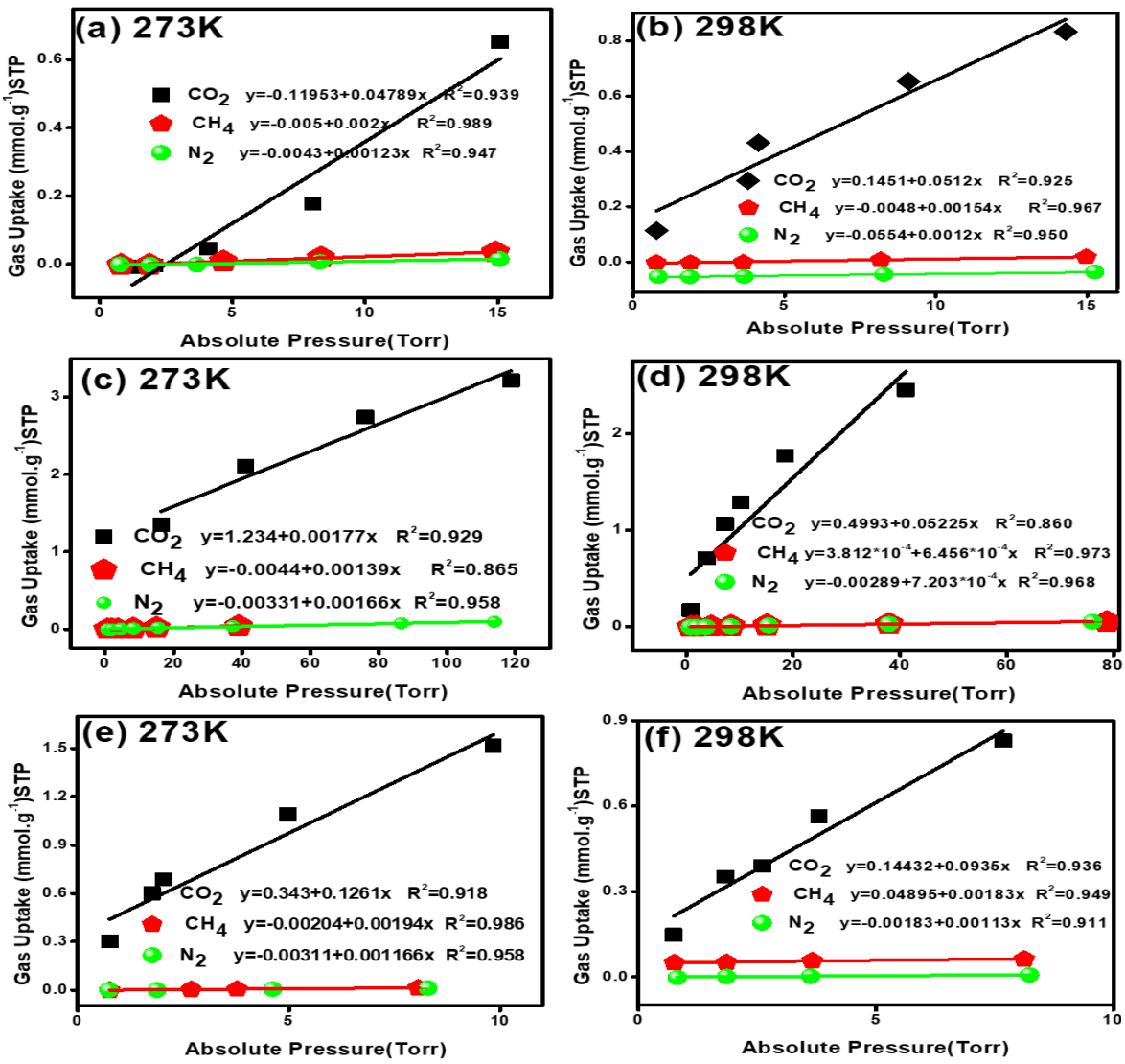

Figure 7. Henry's law initial slope analysis of CO_2, N_2, and CH_4 adsorption isotherms at 273 and 298 K for **(a, b)** YS, **(c, d)** YS/0.2, and **(e, f)** YS/0.5.

The Henry's law constants and the associated ideal selectivities, compiled in Table 8, reveal that glucose modification drastically alters the gas separation behavior of Zeolite Y. For example, at 273 K, the YS sample without any modifications performed the best in terms of CO_2/N_2 and CO_2/CH_4 selectivity's, with the values being 38.93 and 17.61, respectively, whereas for YS/0.2 the values were 10.66 and 12.73. On the other hand, YS/0.5 had the highest CO_2 affinity (KH= 0.1261 $mmol.g^{-1}.bar^{-1}$) and a significantly higher CO_2/CH_4 selectivity of 65.00. Thereby, it can be

inferred that a higher glucose content leads to a greater adsorption of CO_2 relative to CH_4, especially under low-temperature conditions. Different phenomena were detected at 298 K. Both glucose-modified samples outperformed the pristine zeolite. YS/0.2 showed a significant increase in CO_2/N_2 and CO_2/CH_4 selectivity's, reaching 72.54 and 80.93, respectively. YS/0.5, on the other hand, attained the highest CO_2/N_2 selectivity of 82.75 along with a CO_2/CH_4 selectivity of 51.10.

The dramatic rise in selectivity with the temperature going up indicates that the glucose-assisted synthesis probably produced a hierarchical pore structure that allows molecular diffusion and access to the active adsorption sites to be whichever the shortest. The merging of one non-interconnected heterogeneous pore with the structured microporous interior helps the preferential transport and adsorption of the smaller, more polarizable CO_2 molecules while disfavoring the adsorption of N_2 and CH_4. Even if the Henry's constants suggest that the aluminosilicate framework is still the main source of adsorption affinity, the hierarchical modification comes mainly from the better access and use of the high-energy cationic adsorption sites.

The excellent CO_2/CH_4 selectivity of YS/0.2 (80.93) and the maximum CO_2/N_2 selectivity obtained by YS/0.5 (82.75) are clear evidence that the glucose level is a key factor in determining the pore structure and the distribution of the adsorption energy. These results show that glucose-assisted hierarchical modification not only increases the capacity of CO_2 adsorption but also considerably enhances the gas separation performance, rendering the modified Zeolite Y samples as very promising adsorbents for various applications such as post-combustion carbon capture and natural gas purification.

Table 6. Henry constant for gases and selectivity values

Zeolite Type	KH_{CO2}	KH_{N2}	KH_{CH4}	$S_{(CO_2/N_2)}$	$S_{(CO_2/CH4)}$
			273 K		
YS	0.04789	0.00123	0.00272	38.93	17.61

YS/0.2	0.0177	0.00166	0.00139	10.66	12.73
YS/0.5	0.1261	0.001166	0.00194	08.15	65.00
			298 K		
YS	0.0512	0.00122	0.00154	41.97	33.25
YS/0.2	0.05225	7.2030×10^{-4}	6.4562×10^{-4}	72.54	80.93
YS/0.5	0.09351	0.00113	0.00183	82.75	51.10

3.2.3.3 Selectivity models for CO_2 capture evaluation

We compared the selectivity values obtained from the Ideal Adsorbed Solution Theory (IAST) to those derived from Henry's Law constants to evaluate the separation performance of the synthesized Zeolite Y samples. The tables demonstrate the clear variations in the values predicted by these two models. The given tables' data present remarkable divergences in the values foreseen by these two models. By their ratio of Henry's constants, the Henry's Law-based selectivity generally yields much higher figures than the IAST-based technique. It is common as Henry's Law constants are attributed to the low-pressure, infinite-dilution limit whereby adsorption sites are postulated as non-competitive. Although such figures help to quantify the intrinsic thermodynamic affinity of the zeolite surface for specific gas molecules, they often overestimate the separation potential of the substance in a real-world application. Conversely, the IAST-based selectivity better forecasts the situation by considering the competitive adsorption conduct in multi-component systems, therefore reflecting site occupancy at higher gas loads. Noteworthy disparities observed (such the YS/0.2 sample presenting an IAST-based CO2/N2 selectivity of 11.63 as against a Henry's Law-based value of 72.54) illustrate that the latter does not factor in the competitive interactions that limit separation efficiency in a real gas flow. Thus, as the Henry's Law method is a good measure for initial gas-surface affinity, the IAST-based data better capture the real-world performance of these adsorbents in carbon capture applications. Especially in the YS/0.2 sample, moderate glucose modification helps to better capture CO_2 by optimizing the trade-

off between surface functionality and pore interconnectivity, therefore enhancing performance. These findings illustrate the need of evaluating the industrial viability of altered zeolites for gas separation by means of competitive adsorption models. Finally, although Henry's Law constants offer crucial insight into the elementary binding affinities of clean and glucose-altered Zeolite Y, they reflect an optimal limit underestimating the effect of site competition. On the other hand, the IAST analysis offers a more reasonable evaluation of the adsorbent's performance amidst competitive situations. Therefore, we highlight the selectivity derived from IAST as the main measure to judge these materials' fitness for industrial carbon capture, as this technique better captures the complicated gas-pore interactions intrinsic in hierarchical zeolite frameworks.

3.2.3 Thermodynamic Analysis of Gas Adsorption

An important thermodynamic parameter, the heat of adsorption quantifies the strength of the interaction between the molecules of the adsorbate and the adsorbent's surface and can provide a profound analysis concerning the adsorption behavior and adsorbent affinity. Using Equation (2) as expounded before, the adsorption behavior of CO_2, N_2, and CH_4 on unadulterated and glucose-modified Zeolite Y samples was investigated to elucidate such interactions. The isotherms of adsorption at 273.15 K and 298.15 K were used to calculate the isosteric heat of adsorption by extrapolating the relevant equilibrium pressures corresponding to fixed adsorption loadings as depicted in Figure 8. Such fixed adsorption loadings assure thermodynamic consistency and facilitate a reliable comparison of the adsorption behavior at different temperatures as documented in several previous studies [44, 45]. This procedure provides precious insight into the adsorption mechanism and the adsorbent affinity of the synthesized zeolites toward the studied gases.

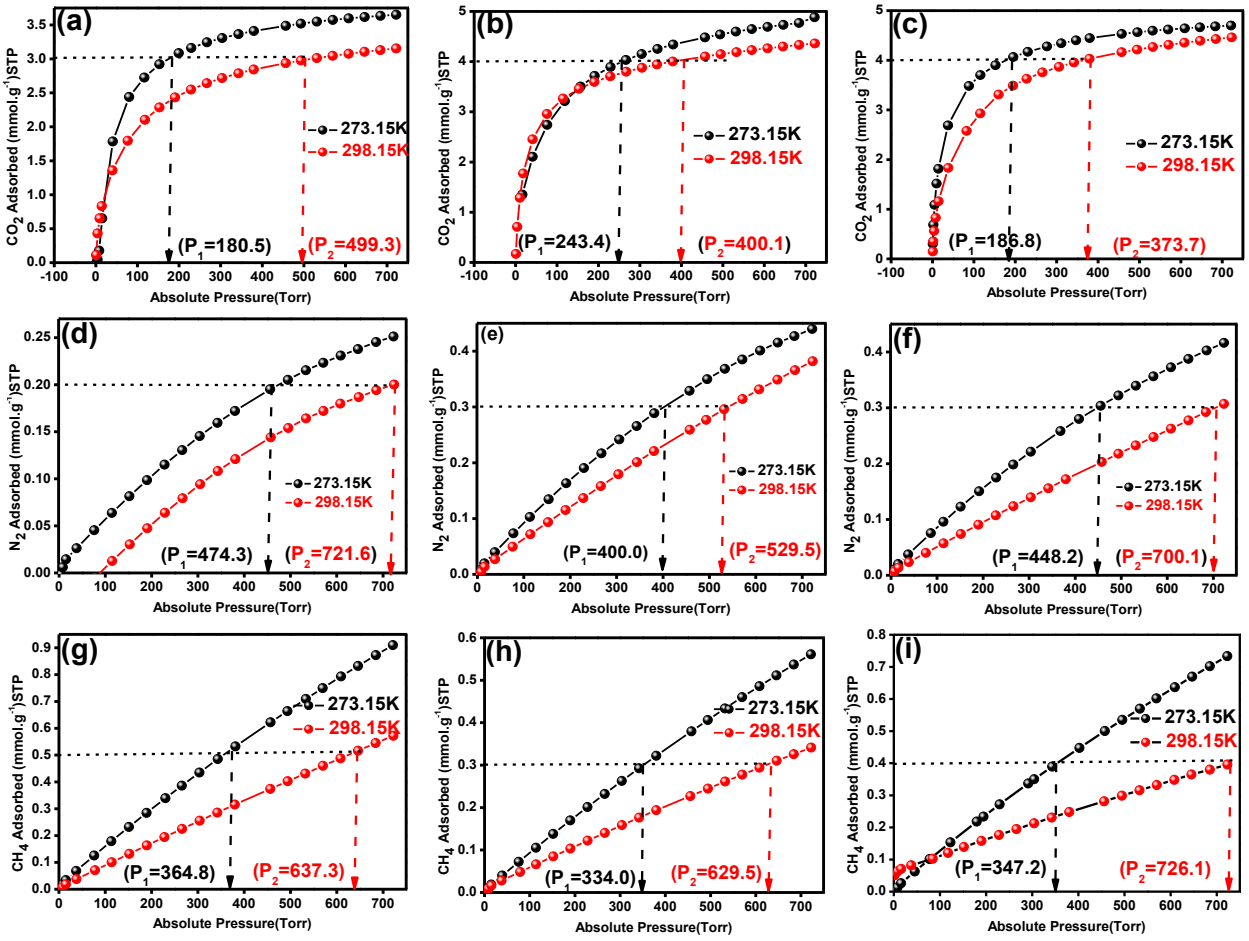

Figure 8. Equilibrium pressures extracted at fixed adsorption loadings from the adsorption isotherms of **(a, b, c)** CO_2, **(d, e, f)** N_2 and **(g, h, i)** CH_4 at different temperatures.

For the determination of the isosteric heat of adsorption, representative adsorption capacities were selected from the measured isotherms for each gas and zeolite samples. For CO_2, adsorption capacities of 3.0 mmol g^{-1} for YS and 4.0 mmol.g^{-1} for both YS/0.2 and YS/0.5 were considered. At these uptake levels, the corresponding pressures obtained from the adsorption isotherms were 180.5 and 499.3 Torr for YS, 243.4 and 400.1 Torr for YS/0.2, and 186.8 and 373.7 Torr for YS/0.5 at 273.15 K and 298.15 K, respectively. For N_2, uptake values of 0.20 mmol.g^{-1} for YS and 0.30 mmol.g^{-1} for both modified samples were selected. The associated pressures were determined to be 474.3 and 721.6 Torr for YS, 400.0 and 529.5 Torr for YS/0.2, and 448.2 and 700.1 Torr for

YS/0.5 at the two investigated temperatures. In the case of CH_4, adsorption capacities of 0.50, 0.30, and 0.40 mmol.g^{-1} were chosen for YS, YS/0.2, and YS/0.5, respectively. The corresponding pressure values were found to be 364.8 and 637.3 Torr for YS, 334.0 and 629.5 Torr for YS/0.2, and 347.2 and 726.1 Torr for YS/0.5 at 273.15 K and 298.15 K, respectively. The equilibrium pressures corresponding to constant adsorption loadings were extracted from the adsorption isotherms and are presented in Figure 9 and summarized in Table 7.

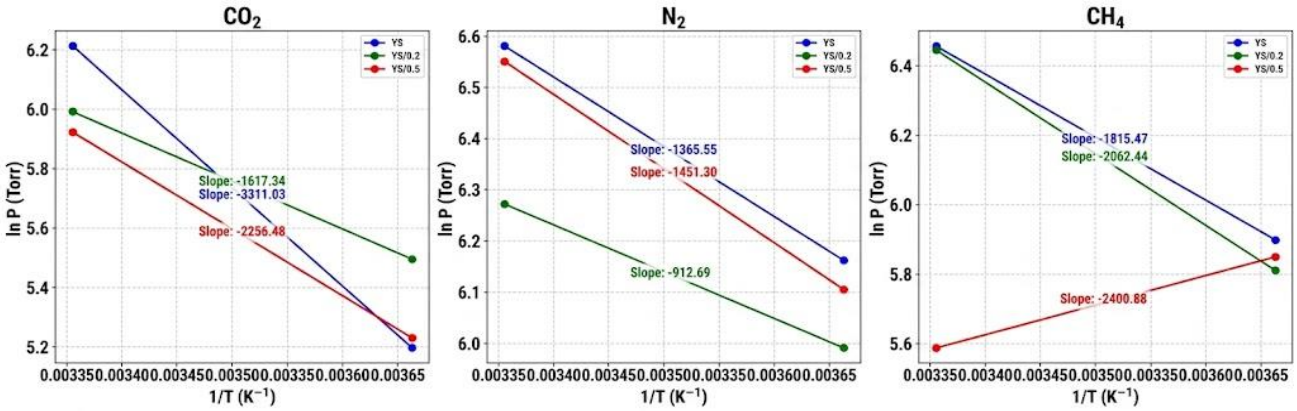

Figure 9. Isosteric heat of adsorption analysis (ΔH_{ads}) via Clausius-Clapeyron plots for Gases on the Three zeolite samples.

Using the Clausius-Clapeyron equation, the adsorption energetics of CO_2, N_2, and CH_4 were evaluated by plotting the natural logarithm of equilibrium pressure (lnP) against reciprocal absolute temperature (1/T), as shown in Figure 9. Following this, the isosteric heat of adsorption (ΔH_{ads}) was found by means of the linear regression slope of every plot, with slope = -ΔH_{ads}/ R. Table 7 presents these derived slopes and the related computed adsorption heats for every zeolite sample.

Table 7. Adsorption heat of gases using unaltered and glucose-modified Zeolite Y samples at various temperatures

Zeolite Type	Gas	Absorbed amount (mmol. g^{-1})	Absolute Pressure (Torr)	Ln(P)	Slope	ΔH_{des} (kJ.mol^{-1})

			P_1 (273K)	P_2 (298K)	$Ln(P_1)$ $LnP_{(273)}$	$Ln(P_2)$ $LnP_{(298)}$		
YS		3.00	180.5	499.3	5.196	6.213	-3311.03	27.53
YS/0.2	CO_2	4.00	243.4	400.1	5.495	5.992	-1617.34	13.45
YS/0.5		4.00	186.8	373.7	5.230	5.923	-2256.48	18.76
YS		0.20	474.3	721.6	6.162	6.581	-1365.55	11.35
YS/0.2	N_2	0.30	400.0	529.5	5.991	6.272	-912.69	7.59
YS/0.5		0.30	448.2	700.1	6.105	6.551	-1451.30	12.07
YS		050	364.8	637.3	5.899	6.457	-1815.47	15.09
YS/0.2	CH_4	0.30	334.0	629.5	5.811	6.445	-2062.44	17.15
YS/0.5		0.40	347.2	726.1	5.850	5.588	-2400.88	19.96

Among the examined gases, the determined adsorption heats show that CO_2 interacts most strongly with the zeolite framework. With 27.53 kJ.mol^{-1}, unmodified zeolite (YS) showed the highest CO_2 heat of adsorption; YS/0.5 (18.76 kJ.mol^{-1}) came next, then YS/0.2 (13.45 kJ.mol^{-1}). These values, which normally correspond with physisorption, confirm that strong physical interactions rather than chemical bonding mostly control CO_2 adsorption. On the other hand, N_2 showed the lowest heats of adsorption (7.59 to 12.07 kJ.mol^{-1}), hence mild interactions with the zeolite surface are indicated. Methane showed middle values of 15.09 to 19.96 kJ.mol^{-1}, which shows better adsorption than N_2 but lesser affinity than CO_2. Overall, the higher Q_{st} values obtained for CO_2 confirm the preferential adsorption of carbon dioxide over N_2 and CH_4 , supporting the suitability of the synthesized composite Zeolite Y with Glucose materials for selective CO_2 capture and gas separation Isotherm Models applications.

3.2.4 Isotherm Models of CO_2 by the Modified Zeolithe Y

The equilibrium adsorption behavior of CO_2 on Ys/0.2 an optimum sample of syntheses zeolites with glucose at 273.15 K was analyzed using three widely adopted isotherm models, namely Langmuir, Freundlich, and Toth. The linear and unlinered fitting results, along with the corresponding model parameters and regression coefficients, are summarized in Table 8, while the agreement between experimental data and model predictions is plotted in Figure 10. Among the examined models, The Langmuir model provided a good fit to the experimental data, with a

correlation coefficient (R^2 = 0.986) and a maximum monolayer adsorption capacity (Q_m) of 5.15 mmol.g^{-1}. At 4.88 mmol.g^{-1}, the expected value is in good agreement with the experimentally measured CO_2 absorption, therefore suggesting that monolayer adsorption on reasonably consistent adsorption sites adds much to the adsorption process. The Langmuir affinity constant ($K_L = 1.15 \times 10^{-2}$ $Torr^{-1}$) also indicates that CO_2 molecules interact well with the zeolite surface. Among the studied models, the Freundlich model had the least fitting accuracy (R^2=0.959) yet it nevertheless well reflected the adsorption behavior. With n = 3.21 and K_F = 0.668, the Freundlich constants point to a positive adsorption process whereby the criteria n > 1 acts as experimental proof of strong interactions between the adsorbent surface and the adsorbate. Moreover, the good fit to the Freundlich model suggests that the adsorbent surface shows structural inhomogeneity and a wide range of adsorption energies.

Table 8. Isotherm models of CO_2 uptake by YS/0.2 constants and parameters

SN	Isotherm Model	Coefficient Constant (R^2)	Constant Parameter	Values	Units
1	Langmuir	0.997	Q_e K_L	5.18 0.0169	mmol. g^{-1}.$Torr^{-1}$
2	Freundlich	0.956	n K_F	3.38 0.744	— mmol. g^{-1}. $Torr^{-1}$
3	Toth	0.999	Q_e t b_T	6.38 0.563 0.0323	mmol.g^{-1} — $Torr^{-1}$

The Toth isotherm gave the best fit of the experimental data among the three models with the highest correlation coefficient (R^2 = 0.999). The adjusted Toth values were q_m = 6.39 mmol.g^{-1}, t = 0.563, and b_T = 0.0323 $Torr^{-1}$. Rising above the quantitatively measured uptake of 4.88 mmol.g^{-1}, the theoretical maximum capacity of the adsorbent under ideal saturation circumstances is shown by the Toth adsorption capacity. The heterogeneity parameter (t = 0.563) shows that the adsorption surface differs from the ideal presumptions of the Langmuir model and is energetically varied.

This finding fits with the structural changes brought about by glucose-assisted synthesis, which created a range of adsorption sites having varied energy profiles.

At last, the adsorption isotherm data show that CO_2 adsorption on the glucose-modified Zeolite Ys/0.2 takes place on a varied surface with non-uniform adsorption sites. The Toth model gave the best fit ($R^2 = 0.999$), therefore confirming its applicability for characterizing the adsorption equilibrium behavior of the created adsorbent even if the Langmuir model correctly predicted the experimental uptake 5.15 vs. 4.88 $mmol.g^{-1}$.

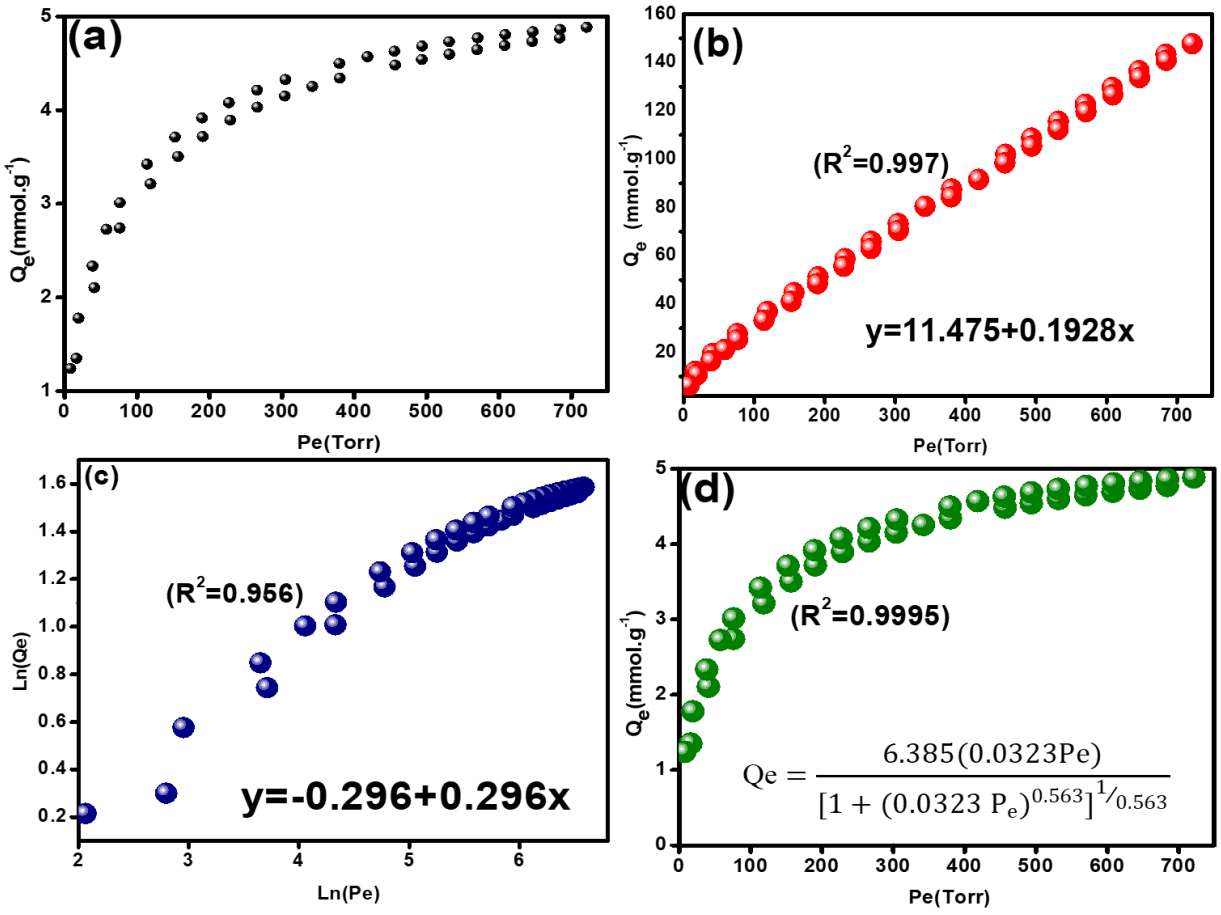

Figure 10. YS/0.2's CO_2 adsorption isotherm at 273.15 K **(a)** Experimental Data with the fitted models **(b)** Langmuir (c) Freundlich and **(d)** Toth

3.2.5 Benchmarking CO_2 Adsorption

Table 9 contrasts the CO_2 adsorption capacity of our created glucose-modified Zeolite Y against several known zeolite-based adsorbents. Our materials demonstrate highly competitive uptake capacities of 4.88 $mmol.g^{-1}$ (YS/0.2) and 4.71 $mmol.g^{-1}$ (YS/0.5) at 1.0 bar and 273 K. This performance is remarkably consistent with the highest reported values for Na-FAU and Na-LTA zeolites (4.60 to 4.96 $mmol.g^{-1}$), confirming that our glucose-mediated synthesis successfully preserves the inherent high-affinity adsorption sites of the Faujasite framework while simultaneously introducing beneficial hierarchical porosity. Both glucose-modified samples much exceed traditional options compared to other frameworks, such MOR (1.05 $mmol.g^{-1}$), ZSM-5 (1.45 to 2.76 $mmol.g^{-1}$), and several Na-CHA structures (2.10 to 3.60 $mmol.g^{-1}$). In addition, it is worthy of note that our method is superior to the raw YS (3.65 $mmol.g^{-1}$) and also keeps up with the conventional Na-A zeolite (3.80 $mmol.g^{-1}$). The enhanced accessibility to pores, the optimized surface functionality in association with the great super cage architectures of the Y-framework, which are all capable of facilitating the effective CO_2 diffusion without the blocking of pores commonly involved in the aggressive chemical modifications such as amine functionalization or alkali treatment, contribute to this enhanced absorption capacity. All the above-mentioned criteria have confirmed the simplicity, sustainability as well as the outstanding success of glucose-mediated hierarchical synthesis in generating high-capacity adsorbents applicable to practical CO_2 capture.

Table 9. Comparative CO_2 Adsorption Performance of Zeolite-Based Adsorbents

No.	Zeolite Type	Activation Agent / Modification	Operating Condition	CO_2 Uptake ($mmol.g^{-1}$)	Ref.
1	MOR Zeolite	None	1.0 bar, 298 K	1.05	[47]
2	Zeolite ZSM-5	NH_4	1.0 bar, 298 K	1.45	[52]
3	Na-ZSM-5	None	1.0 bar, 298 K	2.10	[53]

4	K-CHA	None	1.0 bar, 298 K	2.10	[54]
5	Untreated Na-A	None	1.0 bar, 298 K	2.69	[50]
6	Zeolite ZSM-5	TPAOH	1.0 bar, 298 K	2.76	[51]
7	Zeolite T	TMAOH	1.0 bar, 313 K	3.21	[48]
8	Na-CHA-25	None	1.0 bar, 298 K	3.60	[55]
9	YS	None	1.0 bar, 273 K	3.65	Present
10	Na-A Zeolite	None	1.0 bar, 298 K	3.80	[49]
11	Zeolite T	TMAOH	1.0 bar, 298 K	3.94	[48]
12	Na-FAU Zeolite	None	1.0 bar, 273 K	4.60	[46]
13	YS/0.5	Glucose (0.5 g)	1.0 bar, 273 K	4.71	Present
14	Zeolite T	TMAOH	1.0 bar, 288 K	4.81	[48]
15	YS/0.2	Glucose (0.2 g)	1.0 bar, 273 K	4.88	Present
16	Na-LTA Zeolite	None	1.0 bar, 273 K	4.96	[46]

3.2.6 Impact of Glucose Modification on CO_2 Adsorption

As evidenced by the values provided in Table 4, the CO_2 adsorption capability of Zeolite Y was significantly enhanced by glucose modification. The untreated zeolite (YS) exhibited an adsorption capability of 3.154 mmol. g^{-1}, whereas for the YS/0.2 sample, it was found to increase to 4.526 mmol.g^{-1}. This trend reflects the sensitivity of the performance of the zeolite towards the quantity of modifying agent.

The enhanced performance of YS/0.2 arises from the synergy between moderate glucose addition on surface and textural features. An adequate characterization suggests that the glucose-aided therapy will optimize the pore accessibility and promote the evolution of additional oxygen-containing functional groups. The enhanced pore connectivity facilitates the enhanced transportation across the internal microporous network, whereas the former surface modifications presumably enhance the local electrostatic interactions between the zeolite surface and the CO_2 molecules. Therefore, the moderate change provides an ideal environment for CO_2's sequestration and diffusion. However, the slight loss in capacity observed for YS/0.5 (4.312 mmol.g^{-1}) indicates the presence of an optimum glucose loading threshold. The excessive incorporation of glucose content probably triggers the formation of residual carbonaceous materials to partially plug the

pores or mask the active adsorption sites. Such physical obstruction hinders the internal diffusion pathways, thereby, nullifying the surface-level advantages accrued during the modification process. Collectively, these results indicate that

glucose modification is an effective strategy to tailor the surface chemistry of Zeolite Y for enhanced CO_2 capture, but the concentration needs to be regulated carefully. According to the statistics, moderate glucose

incorporation yields the most desirable trade-off between the maintenance of the structural integrity of the pore network and the optimization of active site availability.

4 POTENTIAL COST-EFFECTIVENESS AND SUSTAIMABILITY ASSESSMENT

The practical application of an adsorbent for carbon capture is dependent on its adsorption ability as well as the simplicity, sustainability, and potential cost-effectiveness of the synthesis method. In this study, zeolite Y was synthesized using easily accessible materials and modified with glucose, a low-cost, sustainable, and eco-friendly carbon source. A glucose-assisted strategy provides a facile and sustainable route for developing high-performance adsorbents for CO_2 capture under relatively mild reaction conditions, in contrast to the traditional modification methods which require the use of expensive templates and complicated functionalization processes. The addition of a small amount of glucose (0.2 g) significantly increased the CO_2 adsorption capacity of Zeolite Y from 3.154 to 4.526 mmol-1 (an increase of ~43.5%). This occurred due to the formation of a hierarchical micro-mesoporous structure that improved the accessibility of pores and facilitated CO_2 diffusion into the internal voids of the adsorbent. For hierarchical zeolites, enhanced connectivity of pores reduced the mass-transport limitations within the porous system and, thus, improved the utilization of the internal pore structure.

5 CONCLUDING REMARKS

The use of glucose as a sustainable soft template led to the effective production of micro-mesoporous Zeolite Y, which improved the CO_2 capture. The confirmation of characterization results revealed that the glucose change retained the structure of the zeolite and prompted the formation of a hierarchical micro-mesoporous network along with the improved surface functioning. These structural changes helped CO2 diffusion and increased pore accessibility, hence improving adsorption performance over the pure zeolite. Among the synthesized materials, YS/0.2 had the biggest CO2 adsorption capacity of 4.89 $mmol.g^{-1}$, which is about 34.0% better than the unmodified Zeolite Y (3.65 $mmol.g^{-1}$). The synergistic action of hierarchical pore development and better accessibility of active adsorption sites, which helped CO2 molecules to diffuse and adsorb inside the zeolite structure, was credited for the improved adsorption capability. By contrast, too much glucose loading caused a slight decrease in adsorption capacity, therefore indicating that there is an ideal glucose concentration that maximizes CO2 uptake. The use of glucose as a low-cost and environmentally friendly modifier successfully improved Zeolite Y's pore structure and CO2 adsorption performance without affecting its structural integrity. These results show that simple and potential technique for creating high-performance zeolitic adsorbents for greenhouse gas reduction and carbon capture is glucose-assisted pore engineering.

Competing Interests

The authors declare that they have no competing interests.

Data availability

The data will be made available upon request.

Acknowledgments

The authors gratefully acknowledge the Deanship of Postgraduate Studies and Scientific Research at Majmaah University, Saudi Arabia, for its generous financial support of this research under

Project No. **ICR-2026-XX**. The authors also sincerely thank the Centre for hydrogen and Carbon Management at King Fahd University of Petroleum and Minerals (KFUPM) for providing laboratory facilities and technical support for the synthesis and characterization of the materials used in this study.

REFRENCES

[1] Landry J-S, Matthews HD. Non-deforestation fire vs. fossil fuel combustion: the source of CO₂ emissions affects the global carbon cycle and climate responses. Biogeosciences 2016;13:2137–49. doi:10.5194/bg-13-2137-2016.

[2] Jayakrishnan KU, Bala G, Cao L, Caldeira K. Contrasting climate and carbon-cycle consequences of fossil-fuel use versus deforestation disturbance. Environ Res Lett 2022;17:064020. doi:10.1088/1748-9326/ac69fd.

[3] Panja P. Deforestation, Carbon dioxide increase in the atmosphere and global warming: A modelling study. Int J Model Simul 2021;41:209–19. doi:10.1080/02286203.2019.1707501.

[4] Aliyu M, Abdelhafez A, Said SAM, Habib MA, Nemitallah MA, Mansir IB. Characteristics of Oxyfuel Combustion in Lean-Premixed Multihole Burners. Energy & Fuels 2019;33:11948–58. doi:10.1021/acs.energyfuels.9b02821.

[5] Said SA, Aliyu M, Nemitallah MA, Habib MA, Mansir IB. Experimental investigation of the stability of a turbulent diffusion flame in a gas turbine combustor. Energy 2018;157:904–13. doi:10.1016/j.energy.2018.05.177.

[6] Fan WK, Tahir M. Recent developments in photothermal reactors with understanding on the role of light/heat for CO_2 hydrogenation to fuels: A review. Chem Eng J 2022;427:131617. doi:10.1016/j.cej.2021.131617.

[7] Ahmed Ali K, Ahmad MI, Yusup Y. Issues, Impacts, and Mitigations of Carbon Dioxide Emissions in the Building Sector. Sustainability 2020;12:7427. doi:10.3390/su12187427.

[8] Fan X, Du Y, Luo B, Han W, Niu S, Gu W, et al. Increasing plant diversity to mitigate net greenhouse effect of wastewater treatment in floating constructed wetlands. J Clean Prod 2021;314:127955. doi:10.1016/j.jclepro.2021.127955.

[9] Bhatt H, Davawala M, Joshi T, Shah M, Unnarkat A. Forecasting and mitigation of global environmental carbon dioxide emission using machine learning techniques. Clean Chem Eng 2023;5:100095. doi:10.1016/j.clce.2023.100095.

[10] Park M, Kwon S, Park J, Jo J, Yoo Y, Kang D. Tailoring the characteristics of deep eutectic solvents comprising quaternized linear polyamine based on the order of amines for CO_2 capture. Chem Eng J 2023;468:143552. doi:10.1016/j.cej.2023.143552.

[11] Ighalo JO, Dulta K, Kurniawan SB, Omoarukhe FO, Ewuzie U, Eshiemogie SO, et al. Progress in Microalgae Application for CO_2 Sequestration. Clean Chem Eng 2022;3:100044. doi:10.1016/j.clce.2022.100044.

[12] Saravanan A, Senthil kumar P, Vo D-VN, Jeevanantham S, Bhuvaneswari V, Anantha Narayanan V, et al. A comprehensive review on different approaches for CO_2 utilization and conversion pathways. Chem Eng Sci 2021;236:116515. doi:10.1016/j.ces.2021.116515.

[13] Rivero J, Lieber A, Snodgrass C, Neal Z, Hildebrandt M, Gamble W, et al. Demonstration of direct ocean carbon capture using hollow fiber membrane contactors. Chem Eng J 2023;470:143868. doi:10.1016/j.cej.2023.143868.

[14] Gupta A. Climate Change and Kyoto Protocol. Handb. Environ. Sustain. Financ., Elsevier; 2016, p. 3–23. doi:10.1016/B978-0-12-803615-0.00001-7.

[15] Zhang R, Liu R, Barzagli F, Sanku MG, Li C, Xiao M. CO_2 absorption in blended amine solvent: Speciation, equilibrium solubility and excessive property. Chem Eng J

2023;466:143279. doi:10.1016/j.cej.2023.143279.

[16] Kong D, Wang S, Luo K, Xu Q, Fan J. Insights of biomass gasification combined with CO_2 absorption enhanced reforming in an 8 MWth dual fluidized bed. Chem Eng J 2023;466:142981. doi:10.1016/j.cej.2023.142981.

[17] Clatworthy EB, Ghojavand S, Guillet-Nicolas R, Gilson J-P, Llewellyn PL, Nesterenko N, et al. Dynamic adsorption of CO_2 by CHA zeolites – Size matters. Chem Eng J 2023;471:144557. doi:10.1016/j.cej.2023.144557.

[18] Abdelnaby MM, Aliyu M, Nemitallah MA, Alloush AM, Mahmoud E-HM, Ossoss KM, et al. Design and Synthesis of N-Doped Porous Carbons for the Selective Carbon Dioxide Capture under Humid Flue Gas Conditions. Polymers (Basel) 2023;15:2475. doi:10.3390/polym15112475.

[19] Kim Y, Lee J, Cho H, Kim J. Novel cryogenic carbon dioxide capture and storage process using LNG cold energy in a natural gas combined cycle power plant. Chem Eng J 2023;456:140980. doi:10.1016/j.cej.2022.140980.

[20] Lively RP, Koros WJ, Johnson JR. Enhanced cryogenic CO_2 capture using dynamically operated low-cost fiber beds. Chem Eng Sci 2012;71:97–103. doi:10.1016/j.ces.2011.11.042.

[21] Janakiram S, Santinelli F, Costi R, Lindbråthen A, Nardelli GM, Milkowski K, et al. Field trial of hollow fiber modules of hybrid facilitated transport membranes for flue gas CO_2 capture in cement industry. Chem Eng J 2021;413:127405. doi:10.1016/j.cej.2020.127405.

[22] Park C-Y, Kong C-I, Kim E-Y, Lee C-H, Kim K-S, Lee J-H, et al. High-flux CO_2 separation using thin-film composite polyether block amide membranes fabricated by transient-filler treatment. Chem Eng J 2023;455:140883. doi:10.1016/j.cej.2022.140883.

[23] Aliyu M, Nemitallah MA, Said SAM, Abdelhafez A, Mansir IB, Habib MA. Role of Adiabatic Flame Temperature on Controlling Operability of a Micromixer-Based Gas Turbine Combustor Holding Premixed Oxy-Flames for Carbon Capture. J Energy Resour Technol 2022;144:1–15. doi:10.1115/1.4053983.

[24] Aliyu M, Abdelhafez A, Nemitallah MA, Said SAM, Habib MA. Effects of adiabatic flame temperature on flames' characteristics in a gas-turbine combustor. Energy 2022;243.

[25] Aliyu M, Nemitallah MA, Said SA, Habib MA. Characteristics of H_2-enriched CH_4-O_2 diffusion flames in a swirl-stabilized gas turbine combustor: Experimental and numerical study. Int J Hydrogen Energy 2016;41:20418–32. doi:10.1016/j.ijhydene.2016.08.144.

[26] Yoro K, Sekoai P. The Potential of CO2 Capture and Storage Technology in South Africa's Coal-Fired Thermal Power Plants. Environments 2016;3:24. doi:10.3390/environments3030024.

[27] Figueroa JD, Fout T, Plasynski S, McIlvried H, Srivastava RD. Advances in CO_2 capture technology—The U.S. Department of Energy's Carbon Sequestration Program. Int J Greenh Gas Control 2008;2:9–20. doi:10.1016/S1750-5836(07)00094-1.

[28] Vorokhta M, Kusdhany MIM, Vörös D, Nishihara M, Sasaki K, Lyth SM. Microporous carbon foams: The effect of nitrogen-doping on CO_2 capture and separation via pressure swing adsorption. Chem Eng J 2023;471:144524. doi:10.1016/j.cej.2023.144524.

[29] Deng Q-F, Liu L, Lin X-Z, Du G, Liu Y, Yuan Z-Y. Synthesis and CO_2 capture properties of mesoporous carbon nitride materials. Chem Eng J 2012;203:63–70. doi:10.1016/j.cej.2012.06.124.

[30] Liu X, Zhou Y, Wang C-L, Liu Y, Tao D-J. Solvent-free self-assembly synthesis of N-doped ordered mesoporous carbons as effective and bifunctional materials for CO_2 capture

and oxygen reduction reaction. Chem Eng J 2022;427:130878. doi:10.1016/j.cej.2021.130878.

[31] Najafi AM, Soltanali S, Ghassabzadeh H. Enhancing the CO_2, CH_4, and N_2 adsorption and kinetic performance on FAU zeolites for CO_2 capture from flue gas by metal incorporation technique. Chem Eng J 2023;468:143719. doi:10.1016/j.cej.2023.143719.

[32] Wang L, Liu J, Lin C, Shang H, Yang J, Li L, et al. Effects of different alkali metal cations in FAU zeolites on the separation performance of CO_2/N_2O. Chem Eng J 2022;431:134257. doi:10.1016/j.cej.2021.134257.

[33] Yue B, Lian X, Liu S, Wu G, Xu J, Li L. Efficient nitrous oxide capture by cationic forms of FAU and CHA zeolites. Chem Eng J 2023;462:142300. doi:10.1016/j.cej.2023.142300.

[34] Azambre B, Chebbi M, Hijazi A. Effects of the cation and Si/Al ratio on CH3I adsorption by faujasite zeolites. Chem Eng J 2020;379:122308. doi:10.1016/j.cej.2019.122308.

[35] Jena KK, Suresh Kumar Reddy K, Karanikolos GN, Alhassan SM. Structure-property relationship of zeolite-Y/cubic ZnS nanohybrid material and its utilization for gaseous phase mercury removal. Chem Eng J 2023;469:143771. doi:10.1016/j.cej.2023.143771.

[36] Dabbawala AA, Ismail I, Vaithilingam B V., Polychronopoulou K, Singaravel G, Morin S, et al. Synthesis of hierarchical porous Zeolite-Y for enhanced CO_2 capture. Microporous Mesoporous Mater 2020;303:110261. doi:10.1016/j.micromeso.2020.110261.

[37] Luzzi E, Aprea P, Salzano de Luna M, Caputo D, Filippone G. Mechanically Coherent Zeolite 13X/Chitosan Aerogel Beads for Effective CO_2 Capture. ACS Appl Mater Interfaces 2021;13:20728–34. doi:10.1021/acsami.1c04064.

[38] Kumar S, Srivastava R, Koh J. Utilization of zeolites as CO_2 capturing agents: Advances and future perspectives. J CO2 Util 2020;41:101251. doi:10.1016/j.jcou.2020.101251.

[39] Asmaly HA, Elbager MA, Ibrahim AI, Nasser GA, Abdelkreem SSE, Al-Suwaiyan M, Elgzoly MAA. Synthesis of chabazite zeolite: A dual-function material for high-performance carbon capture and para-nitrophenol removal from synthetic wastewater with comprehensive characterization and modeling. Chem Eng Sci 2025;121736. doi:10.1016/j.ces.2025.121736.

[40] Alemin, Yahya, et al. "Porosity Engineering and Functionalization of Hyper-Cross-Linked Polymers for Highly Selective CO_2 Adsorption." Macromolecular Rapid Communications 46.14 (2025): 2500020.

[41] Asmaly, H. A., Khalil, A., Hakeem, A. S., & Mohammed, A. M. (2024). Capturing CO_2 through high surface area activated carbon derived from seed shells of Balanites aegyptiaca. Chemistry–An Asian Journal, 19(13), e202400141.

[42] Galanti, M., Teunissen, R., Roghair, I., & van Sint Annaland, M. (2026). Toward consistent thermodynamic modeling of CO_2 adsorption on Lewatit VPOC 1065 under dry conditions: isotherm variability, data gaps, and model fitting. Current Opinion in Chemical Engineering, 51, 101201.

[43] Das M, Klunk MA, Srivastava A, et al. Sustainable fabrication of zeolite Y from rice husk ash and metakaolin for the adsorption of Rhodamine B dye. Chem Pap 2026;80:3009–3023. doi:10.1007/s11696-025-04568-6.

[44] Asmaly HA, Elbager MA. Enhanced CO_2 capture using sustainable biomass-derived activated carbon from desert date seed husk: Adsorption isotherms, selectivity, and RSM optimization. J CO_2 Util 2026. doi:10.1016/j.jcou.2026.103411.

[45] Elbager MA, Asmaly HA, Al-Suwaiyan M, Saleh TA. Transforming palm waste into poly(acrylamide-acrylic acid)-modified green carbon fibers: A sustainable high-

performance adsorbent for CO_2 capture. Biomass Bioenergy 2026;208:108784. doi:10.1016/j.biombioe.2025.108784.

[46] Bénariac-Doumal L, Deroche I, Nouali H, Paillaud J-L, Ors T, et al. A comparative study of CO_2 adsorption in a series of zeolites. Phys Chem Chem Phys 2025;27(20):10621–10634. doi:10.1039/D5CP00538H.

[47] Li, D., Lu, X., Chokkalingam, A., & Iyoki, K. (2025). Capture of Low-concentration Carbon Dioxide with Ultrafast-synthesized MOR-type Zeolites as Adsorbents. https://doi.org/10.26434/chemrxiv-2025-mqhbd.

[48] Jiang, Q., Rentschler, J., Sethia, G., Weinman, S., Perrone, R., & Liu, K. (2013). Synthesis of T-type zeolite nanoparticles for the separation of CO_2/N_2 and CO_2/CH_4 by adsorption process. Chemical Engineering Journal, 230, 380-388.

[49] Xia, H., Hu, Y., Bao, Q., Zhang, J., Sun, P., Liang, D., & Wang, X. (2023). Adsorption separation of O_2/N_2 by Li-RHO zeolite with high oxygen selectivity. Microporous and Mesoporous Materials, 350, 112442.

[50] Shui, L., Zhou, J., Wang, Y., & Lin, Y. (2025). Facile method for enhancing the CO_2 adsorption capacity of zeolites through vacuum-assisted alkaline treatment. RSC advances, 15(25), 19802-19809.

[51] Yan, X. H., Li, P., Yuan, H., Huang, W., Hu, Z., & Yang, R. T. (2025). CO_2 capture by ZSM-5 with varied Si/Al molar ratios: Isothermal adsorption capacity of CO_2 vs dynamic CO_2 adsorption capacity. Separation and Purification Technology, 354, 129304.

[52] Al-Mamoori, A., Saed, U. A., Saoud, A. A., Abdul Jabbar, M. F., Jasim, A., Majdi, H. S., ... & Iacomi, P. (2025). Modification of the zeolite ZSM-5 adsorbent for CO_2 capture. ACS

omega, 10(20), 20129-20141.

[53] Couck, S.; Lefevere, J.; Mullens, S.; Protasova, L.; Meynen, V.; Desmet, G.; Baron, G. V.; Denayer, J. F. M. CO_2 , CH_4 and N_2 Separation with a 3DFD-Printed ZSM-5 Monolith. Chem. Eng. J. 2017, 308, 719−726.

[54] Shang, J., Li, G., Singh, R., Gu, Q., Nairn, K. M., Bastow, T. J., ... & Webley, P. A. (2012). Discriminative separation of gases by a "molecular trapdoor" mechanism in chabazite zeolites. *Journal of the American Chemical Society*, *134*(46), 19246-19253.

[55] Guo, Y., Sun, T., Gu, Y., Liu, X., Ke, Q., Wei, X., & Wang, S. (2018). Rational synthesis of chabazite (CHA) zeolites with controlled Si/Al ratio and their $CO_2/CH_4/N_2$ adsorptive separation performances. *Chemistry–An Asian Journal*, *13*(21), 3222-3230.